Study of Metallurgical Phenomena in the HAZ of 6061-T6 Aluminum Welded Joints

An area of minimum hardness in the HAZ appears to be the location of initial failure regardless of welding variables

BY V. MALIN

ABSTRACT. The interrelationships between welding variables, peak temperatures, microhardness, dilution, microstructure, failure location and strength of gas metal arc (GMA) welded joints in extruded aluminum Alloy 6061-T6 in the heat-affected zone (HAZ) and at the weld interface (fusion line) were investigated. The experimental data obtained have a good correlation with precipitate distribution reported in the literature. Extruded test panels were welded using pulsed GMAW and varying welding parameters. Microhardness and peak temperatures were measured across the welded joints, which were subjected to tensile tests. Several typical hardness areas were identified in the welded joint. In the HAZ, starting from the base metal and moving toward the weld interface, Area 1 was characterized by lower hardness and the presence of local soft spots. This region was followed by Areas 2 and 3 characterized by a significant reduction and recovery of hardness, respectively. This resulted in a plane of minimum hardness within the HAZ where hardness may be as low as 50–60% of that for the base metal. Failure during tensile testing typically occurred through this region regardless of the welding variables used. Areas 4 and 5 were revealed on both sides of the weld interface, which have not been reported in prior literature. In Area 4 on the side of the base metal, less than 0.020 in. (0.5 mm) from the weld interface, hardness also decreased dramatically. In Area 5 in the fusion region, hardness recovered even more dramatically. This created another plane exhibiting very low hardness. Some of the failures during tensile testing occurred in this region. The peak temperature profiles were measured in the HAZ and compared with the corresponding hardness profiles. It was found that the minimum hardness and the location of failure of the tensile specimens in the HAZ occurred in the region subjected to a temperature of 716°F (380°C). This turned out to be the upper limit of existence of B″ phase, the basic strengthening precipitate in Alloy 6061-T6. The greatest effect on hardness and strength of the welded joints was found to be in a critical zone of the HAZ (sometimes called overaged zone in literature) subjected to peak temperatures of 464°–716°F (240°–380°C), the temperature interval (ΔT_B) of existence of the B′ phase precipitate. A direct relationship between average peak temperature gradient and average hardness gradient in the critical zone was established. Both gradients have direct correlation with strength of the welded joints. The lower the gradients, the lower the tensile strength. Two main factors were identified which are responsible for loss of hardness and strength in the critical zone: the extent of the zone and the time of its exposure to the critical temperature interval ΔT_B (464°–716°F).

It was found that the strength of the welded joints in Alloy 6061-T6 can be qualitatively determined by the width and location of the critical zone. The narrower the critical zone and the closer this zone to the weld, the higher the strength of the welded joint. A comparative practical test was developed to discriminate welding conditions by determining the width and the location of the critical zone using temperature paints or sticks. The losses of hardness and strength in the HAZ are believed to be a result of coarsening of strengthening B″ phase precipitate and its transformation into B′ phase. The loss of hardness and strength at the weld interface may be a result of a complete dissolution of the precipitates and migration of Mg from the base metal into the weld.

KEY WORDS

HAZ
6061-T6 Aluminum
Aluminum Extrusion
GMAW
Tensile Test
Hardness Test
Weld Parameters
Peak Temperature
Mechanical Properties
Microstructure

V. MALIN is with BIRL, the industrial research laboratory of Northwestern University, Evanston, Ill.

Introduction

This article describes metallurgical phenomena that were observed in 6061-T6 aluminum welded joints during a program on development of advanced technology for fabrication of extruded

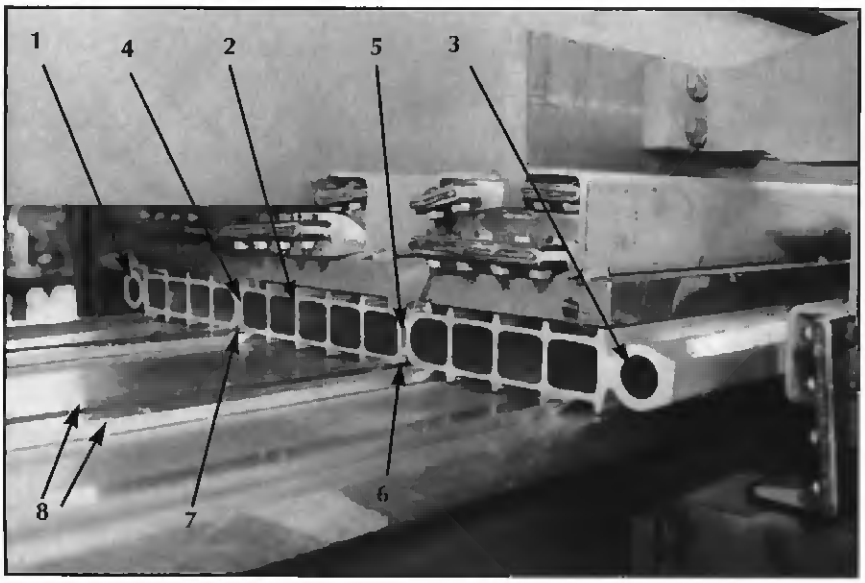

Fig. 1 — A fixture used for assembling extruded mat panels. Legend: 1, 2 and 3 — panels; 4 through 7 — welded joints; 8 — chiller bars.

aluminum roadway mat panels sponsored by the U.S. Army. A wide variety of weldments made of 6061-T6 aluminum extrusions find numerous applications in many industries. However, it has long been known that the heat of welding deteriorates mechanical properties of welded joints in heat-treatable aluminum alloys. This includes loss of hardness and tensile strength in the heat-affected zone (HAZ) of the alloy. The heat-treatable Al-Mg-Si alloys are strengthened by solution and precipitation heat treatments. These treatments usually consist of solutioning, quenching and aging. The main process responsible for this improvement is a formation of second phase precipitates in the aluminum matrix. The precipitates may significantly increase hardness and tensile strength of Al-Mg-Si alloys depending on precipitate structure, size and distribution.

The initial precipitation structure may be profoundly affected by the heat of welding. The resultant deterioration of mechanical and metallurgical properties typical for these alloys is recognized by national standards in many countries. For example, a significant reduction (typically about 43%) in the maximum allowed design stresses is required by the ASME *Pressure Vessel Code*, Section VIII for welded joints in Alloy 6061-T6. A great number of studies have been dedicated to the investigation of precipitate morphology and sequence in Al-Mg-Si alloys; however, very few studies have addressed issues concerning the effect produced by heat of welding on the established microstructure of the alloy. Also, very little is known about how these structural alterations may practically affect HAZ properties of welded joints performed under fabrication conditions. To better understand actual causes, and the nature and magnitude of deterioration of the initial structure and properties of commercial 6061-T6 alloy by heat of welding, hardness profiles of welded joints were studied.

Microhardness has always been a valuable and affordable tool for revealing structural changes in welded joints (Ref. 1). The objectives of this study were to correlate the results of hardness tests with welding conditions (parameters), and physical (temperature) and mechanical (failure location and tensile strength) properties of the welded joints. The attempt was also made to correlate the obtained experimental data with the data on metallurgical (microstructure, precipitate distribution) properties of the HAZ in welded joints reported by other investigators.

Specifics of Precipitation in Commercial 6061 Alloy

A great deal about structural behavior of Al-Mg-Si alloys has been learned over the years by experimenting with alloys in which Mg and Si are present in proportions that provide formation of the equilibrium phase, magnesium silicide (Mg_2Si). In the literature, such alloys, including 6061, are usually referred to as Al-Mg_2Si pseudo-binary alloys to distinguish them from ternary Al-Mg-Si alloys in which the equilibrium proportion is not observed. However, there are several reasons why commercial Alloy 6061 cannot be considered a pure pseudo-binary alloy. The ideal Mg:Si weight ratio (1.73) for Mg_2Si is not practically achieved in commercial 6061 alloy. However, according to Ceresara, *et al.* (Ref. 2), an excess of Mg or Si not exceeding 0.5% (typical for 6061 alloy) affects neither the sequence nor the structure of normal precipitation, but rather its rate and/or extent. Dumolt (Ref. 3) found out that precipitates formed in the later stage of the precipitation sequence in commercial 6061 alloy displayed light structural differences compared to those found in Al-Mg_2Si alloy. Also, a commercial 6061 alloy contains about 0.30 wt-% Cu and 0.2 wt-% Cr. In this respect, the addition of Cu in an amount less than 1% may result in the formation of the quaternary phase, according to Suzuki, *et al.* (Ref. 4).

However, despite these differences, it is widely recognized (Ref. 5) that the general precipitation characteristics and behavior of commercial alloy 6061 are not radically different from those of pseudo-binary Al-Mg_2Si alloys. This allows the data obtained in studying pseudo-binary Al-Mg_2Si alloys, such as precipitation sequence, the precipitate phase characteristics, temperature ranges, and their effect on hardness of the alloy, to be applicable to commercial Alloy 6061 as well. Since these data are scattered in welding literature, the following discussion is intended to introduce the readers to the basics of precipitation hardening in Alloy 6061.

Precipitation Sequence and Its Effect on Hardness in 6061 Alloy

The precipitation sequence for Alloy 6061 is well established in the literature. Despite some ambiguity concerning structure and morphology of some precipitates, the generally recognized (Ref. 6) sequence of metastable phases produced by ternary Al-Mg-Si alloys along the Al-Mg_2Si pseudo-binary line is the following:

$$\alpha' \rightarrow \alpha + \text{G.P.} \rightarrow \alpha + B'' \rightarrow \alpha + B' \rightarrow \alpha + B$$

In this paper, the letter B will be used instead of β, frequently used in the literature to describe the precipitates developed in pseudo-binary alloys. As was already mentioned, some structural differences in the precipitates were found in commercial 6061 alloy by Dumolt (Ref. 3). In order to distinguish these precipitates from those described for pure pseudo-binary alloys, Dumolt identified the precipitates by the letter B. This rule will be followed here as well in describing the precipitates below.

The supersaturated solid solution (α′) is a structure produced by solutionizing and quenching. During solutionizing,

Table 1 — Composition and Properties of Base and Filler Metals

Metal	Element (wt-%) Si	Mg	Cu	Fe	Mn	Zn	Cr	Ti	Al	Strength (avg.) Tensile/Yield ksi	MPa	Elongation in 2 in. max. %
Base 6061	0.68	0.85	0.22	0.32	0.07	0.05	0.06	0.02	Bal	44.35/305.8	41.9/288.9	9
Filler metal 4043	4.80	0.05	0.17	0.24	0.05	0.05	0.05	0.05	Bal	—	—	

the alloy is heated to and held at a temperature just below the eutectic temperature until the equilibrium solid solubility limit is attained. The purpose is to put the maximum practical amount of solutes (Mg and Si) responsible for strengthening into solid solution of the aluminum matrix (α). As a result of quenching (rapid cooling to room temperature), the solid solution becomes supersaturated. The resulting structure (α') is very soft but has a tendency to precipitate the solute that is in excess of the amount soluble at room temperature. This increases hardness and strength of the matrix.

Gunnier-Preston (G.P.) zones are the first product of decomposition of the supersaturated solution. Like all other precipitates, G.P. zones are beyond the resolution of an optical metallograph. According to Panceri, *et al.* (Ref. 7), formation of G.P. zones is detected at temperatures below 320°F (160°C) under isothermal conditions. Lutts (Ref. 8) referred to G.P. formation as "pre-precipitation" or "clustering," meaning that an actual precipitation follows. G.P. zones have not yet been observed via transmission electron microscopy (TEM), but their presence was detected by resistivity measurements by Panceri, *et al.* (Ref. 7), in Al-1.4% Mg_2Si alloy. Since G.P. zones are extremely small in comparison to other precipitates, they are able to make only a modest contribution to strength (mechanical properties) of the material (Ref. 7). This was also confirmed by Enjo, *et al.* (Ref. 9). The morphology of the G.P. zones is thought to be spherical or needle-like, according to Mondolfo (Ref. 6).

The B″ phase is the next phase in the precipitation sequence. It is the first phase visible via TEM. It precipitates as needles, which can grow significantly from 320°F upon continued aging or temperature rise. The solvus temperature of the B″ phase has been reported to be 428°F (220°C) by Thomas (Ref. 10) and 464°F (240°C) by Miyauchi, *et al.* (Ref. 11). Thomas showed that the maximum strengthening in pure Al-0.97%Mg-0.61%Si alloy (Mg_2Si equivalent of 6061) occurs when it is aged to produce a needle structure. This was confirmed by Enjo, *et al.* (Ref. 9), for 6063-T5 alloy. According to Dumolt (Ref. 3), increasing the aging temperature leads to a considerable softening of the alloy due to coarsening of B″ precipitate.

The B′ phase precipitates are next in the sequence. They are described by Thomas (Ref. 10) as rod-shaped particles with a structure corresponding to a highly ordered unit cell of Mg_2Si. Formation of rods occurs from needles (B″ phase) by increases in precipitate length and diameter (Ref. 10). The temperature range of the existence of rods was found to be 464°–716°F (240°–380°C) by Miyauchi, *et al.* (Ref. 11). However, according to Dumolt (Ref. 3), this range is believed to be considerably wider, 662°–860°F (350°–460°C). Transformation of the B″ phase into the B′ phase is associated with softening of the alloy since B″ precipitates contribute more to hardening of the alloy than B′ precipitates, according to Enjo, *et al.* (Ref. 9).

The equilibrium B phase (Mg_2Si) is developed at the final stage of the precipitation sequence. It exists as platelets which grow out of the intermediate rod structure or nucleate independently (Ref. 10). According to Enjo, *et al.* (Ref. 9), Mg_2Si contribution to hardness of the alloy is very small.

Insoluble compounds may be present in commercial 6061 alloy in addition to the precipitates discussed above. These particles were found in the structure at all stages of the precipitation sequence. However, their effect on hardness of the alloy is negligible (Ref. 9).

The conclusion of this review is that the B″ phase produces the greatest effect on strength and hardness of Alloy 6061, while the contribution of the B′ phase is moderate. All the other particles affect hardness very little.

Experimental Procedure

The following materials were used for the experiments: the base metal was in the form of extruded hollow panels in as-received T6 conditions produced from commercial 6061 aluminum alloy; the electrode metal was in the form of a 0.045-in. (1.2-mm) diameter wire produced from Alloy 4043; the shielding gas was pure argon supplied at a flow rate of 32–45 ft^3/h (0.25–0.35 L/s). The nominal alloy compositions of the base and electrode metals are shown in Table 1. The welding process was pulsed gas metal arc welding (GMAW-P). A special rotating fixture, shown in Fig. 1, was used to assemble three 60-in. (152.4-cm) long panels (1–3). Joint configuration was a single-V groove butt joint (Refs. 4–7) having a 60-deg included angle and being 3/16 in. (4.7 mm) deep. The fixture was equipped with special copper chiller bars (Ref. 8) to chill the HAZ on both sides of each weld.

The following variables and their corresponding symbols were used in the discussion below:

I — mean values of welding current (ampere)

U — mean values of voltage (volt)

S — mean values of welding (travel) speed (inch/min or mm/sec) P = I x U - electric power (Kwt)

Q = P/S linear arc energy or heat input (J/in. or J/mm).

The mean values were determined through a computerized statistical analysis of the parameter values sampled 100 times per second by the corresponding sensors during welding.

Electric powers (P) of low, medium and high levels are represented by A, B, and C series of experiments, respectively, as shown in Table 2. Values for P were changed by varying I, U or both. Maximum deviation from average power (P_{ave}) within each P level did not exceed 4%.

Linear arc energies (Q) changed by varying P, S or both. Q values of low (L), medium (M) and high (H) levels were achieved in each series of experiments (Table 2). Values of average linear energy (Q_{ave}) for these Q levels were 12.86 kJ/in. (0.506 kJ/mm), 17.16 kJ/in. (0.676 kJ/mm) and 25.21 kJ/in. (0.992 kJ/mm), respectively. Maximum deviation from Q_{ave}

Table 2 — Welding Conditions

Weld ID	Current I (A)	Voltage U (V)	Power P = IxU (watt)	Travel Speed S (in./min)	(mm/s)	Linear Energy Q = P/S (kJ/in.)	(kJ/mm)	(level)[b]	Dilution Rate (%)
A4[a]	145.68	19.27	2807	13.0	5.5	12.95	0.510	L	39.37
A5	142.11	19.63	2790	13.0	5.5	12.88	0.507	L	22.22
A6	136.62	20.22	2763	9.75	4.12	17.00	0.669	M	18.36
A10	134.35	20.39	2739	6.5	2.75	25.29	0.996	H	16.60
A9	144.82	19.24	2786	19.5	8.25	8.57	0.337	EL	43.14
		Low Pave = 2777							
B16[a]	197.10	21.16	4171	13.0	5.5	19.25	0.758	MH	62.00
B17	184.71	22.39	4136	13.0	5.5	19.09	0.752	MH	36.00
B18	185.78	21.36	3968	9.75	4.12	24.42	0.961	H	34.50
B22	191.59	21.97	4209	14.6	6.18	17.30	0.681	M	37.22
B23	202.04	20.60	4162	19.5	8.25	12.81	0.504	L	54.65
B24	202.03	20.55	4152	26.0	11.0	9.58	0.377	EL	53.30
		Medium Pave = 4133							
C28[a]	241.92	23.03	5571	13.0	5.5	25.71	1.012	H	63.70
C29	249.30	22.10	5510	13.0	5.5	25.43	1.001	H	44.46
C30	228.61	23.87	5457	9.75	4.12	33.58	1.322	EH	37.38
C35	246.04	22.71	5588	19.5	8.25	17.19	0.676	M	59.93
C33	251.70	21.95	5525	26.0	11.0	12.75	0.502	L	54.92
		High Pave = 5530							

a HAZ is not chilled.
b Q levels: L-low, M-medium, H-high, EL-extra low, EH-extra high, MH-medium high.

within each Q level did not exceed 1.5%.

HAZ chilling was utilized for all the welds, with the exception of A4, B16, and C28. These were performed without chilling for comparison with chilled welds A5, B17, and C29.

Tensile tests were conducted on two specimens taken transverse to the weld. They were machined to the thickness slightly below 0.125 in. (3.2 mm), the wall thickness of the panel, as will be shown in the figures below. Average values of tensile strength and failure distances from the weld interface (fusion line) are shown in Table 3.

Microhardness tests were conducted on a cross-section of transverse specimens with a Knoop microhardness tester at 100-g load. Hardness measurements were made across the weld interface parallel and 0.062 in. (1.6 mm) below the face surface of the specimen. The imprints were made with increments of 0.250–0.125 in. (6.4–3.2 mm) in the area away from the weld interface. The increments were reduced to 0.062 in. (1.6 mm) and then to 0.031 in. (0.8 mm) as the weld interface was approached. A relatively small (100-g) load was selected in order to increase resolution of the test. This was instrumental in the areas immediately adjacent to the weld interface where imprints were taken with an increment of 0.005 in. (0.127 mm).

Peak (maximum) temperatures (T_{max}) across the HAZ were measured with the aid of temperature indicating liquid paints. Prior to welding, narrow strips of the paints rated from 200°F (93°C) to 900°F (482°C) were applied by brush to the face surface of the panels perpendicular to the joint to be welded. After drying and welding, the distance was measured from the edge of the weld to the end of the melted portion of the strip where the rated temperature had been reached. Unfortunately, T above 700°F (371°C) could not be reliably determined and therefore were extrapolated to the solidus temperature. The solidus temperature was estimated from Ref. 12 based on 4043 type weld metal composition and a calculated rate of dilution.

Dilution rate (DR) was determined from a macrographic cross-section of a transverse specimen, which was photographed and enlarged by a factor of 10 ± 0.5%. DR was calculated using the formula:

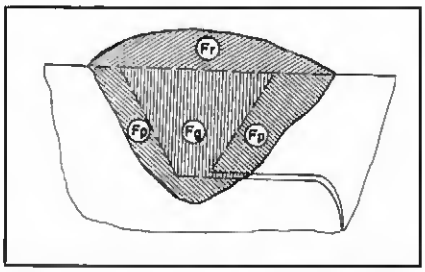

Fig. 2 — Cross-sectional areas of the welded joint. Legend: Fr — joint penetration; Fg — groove, and Fr — reinforcement.

Table 3 — Results of Tensile Tests

Weld ID	Tensile Strength Average (ksi)	(MPa)	Failure[b] Location Face (in.)	Root (in.)	Failure Distance from FL
A4[a]	26.75	184.4	HAZ	0.32–0.36	0.38–0.42
A5	30.30	208.9	W	Center	Center
A6	29.55	203.7	W	Center	Center
A10	29.30	202.0	FL	0.13–0.20	0–0.02
B16[a]	26.0	179.0	HAZ	0.37–0.40	0.48–0.50
B17	31.1	214.4	FL	0.09–0.18	0–0.06
B18	29.9	206.2	HAZ	0.14–0.20	0.28–0.30
B22	31.4	216.5	W/HAZ		
C29	28.55	196.8	FL		
C30	27.45	189.3	HAZ	0.22–0.24	0.37–0.42
C35	30.6	211.0	HAZ		
C33	29.05	200.3	HAZ	0.18–0.22	0.22–0.28

a. HAZ is not chilled.
b. Failure locations: W-weld; FL-fusion line; HAZ-heat-affected zone; W/HAZ-weld (1st specimen), HAZ (2nd specimen).

$$DR = Fp/(Fg+Fr+Fp) \times 100\%$$

where Fp, Fg and Fr are cross-sectional areas (shown in Fig. 2) of arc penetration, groove and weld reinforcement, respectively, measured from the photographs with the aid of a polar planimeter. Calculated values of dilution rates for all welds are included in Table 2.

Results of Experiments

Effect of Weld Storage Period on HAZ Hardness

Effect of weld storage period on heat-affected zone (HAZ) hardness was studied to determine how the variations in storage time may affect the HAZ hardness and possibly the strength of the experimental welds. In heat-treatable Al-Mg-Si alloys, a significant reduction in hardness occurs in the HAZ after welding. It is known (Ref. 13) that natural aging (storing at room temperature) may restore as-welded hardness to a certain degree. To study this phenomenon, four transverse samples were cut adjacent to each other from a welded joint. The samples were tested for microhardness distribution across the HAZ and the minimum hardness in the HAZ was determined after storage periods of 4 h (as-welded condition), 7, 14 and 28 days. As shown in Fig. 3, the minimum hardness in the HAZ recovered 16, 21 and 28% of as-welded hardness after storage for 1, 2 and 4 weeks, respectively. The most rapid hardness recovery occurred in the first week of storage, with an average recovery rate of 2.3% per day. Subsequently, hardness increased at a much lower and ever decreasing rate. For example, during the third and forth weeks of storage, hardness recovered at an average rate of 0.5% per day. In order to minimize the effect of natural aging on the comparative test results of this study, testing was conducted after at least three weeks of storage.

Microhardness Profiles

Analysis of the hardness profiles across the weld interface showed systematically that the HAZ and the weld can be divided into several distinguishable hardness areas. A hardness profile across welded joint B17 is shown in Fig. 4A. Here, hardness values in the HAZ (H_{HAZ}) and in the weld (H_w) are plotted as a function of the distance (D) from the weld interface. For clarity, an actual cross-section of this weld is superimposed on the hardness profile - Fig. 4B.

The base metal (BM) hardness (H_{BM}) was scanned on an unwelded test specimen along the hardness measurement line (Fig. 4B) starting 0.031 in. (1.2 mm) from the groove edge, which is shown by dashed lines. A typical H profile in the BM is shown in Fig. 4A (dashed lines). Here, for Weld B17, an average hardness value $H_{BM\ ave}$ equals to 112 HK, with maximum fluctuations from average being approximately 10%. These fluctuations may be a result of uneven heat treatment due to a nonuniform cross-section of the extruded panel.

The HAZ followed the BM. Moving toward the weld interface, four distinct hardness areas in the HAZ were identified as shown in Fig. 4A by sequential numbers.

Area 1 is characterized by more erratic hardness fluctuation than is observed in the BM. Hardness in this area is lower (down to 24% in this case) than $H_{BM\ ave}$, a decrease of approximately 24% for this particular welded joint. The width of Area 1 (W) was not determined in this study, but the described phenomenon was observed as far as 2 in. (51 mm) away from the weld interface. Lower hardness and the presence of local soft spots did not seem to have significant effect on HAZ properties since failure of tensile test specimens never occurred within this area. However, this may indicate an onset of more profound microstructural changes in the HAZ closer to the weld interface.

Area 2 is characterized by a significant softening of the HAZ. Hardness in this area decreases rapidly to a very low value which may reach 58 HK (48% $HB_{M\ ave}$). The width of this area (W_2) varies in a relatively wide range of 0.187 to 0.688 in. (4.7–17.5 mm) depending on linear energy Q (for Q values see Table 2). For example, for Weld B23 that was chilled and performed at low Q, W_2 was equal to 0.187 in. (4.7 mm), while for Weld B18 that was also chilled and performed at high Q, W_2 was equal to 0.532 in. (13.5 mm), a dramatic 280% increase in width of this area. Chilling of the HAZ reduced W_2, but not that dramatically. For example, for nonchilled Weld A4 and chilled Weld A5 performed at the same low Q, W_2 was measured at 0.412 in. (10.5 mm) and 0.312 in. (7.9 mm), respectively. This represents a reduction of W_2 by 32%. These results indicate that W_2 is strongly affected by the welding thermal cycle.

A useful characteristic of hardness distribution in an area is the average hardness gradient (G_{ave}). It indicates how rapidly the softening or hardening occurs over the width of the area considered:

$$G_{H\ ave} = \Delta H/W$$

where ΔH is the difference between max-

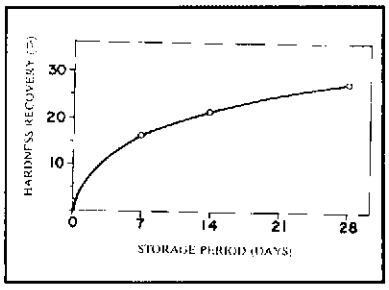

Fig. 3 — Effect of weld storage period on HAZ hardness.

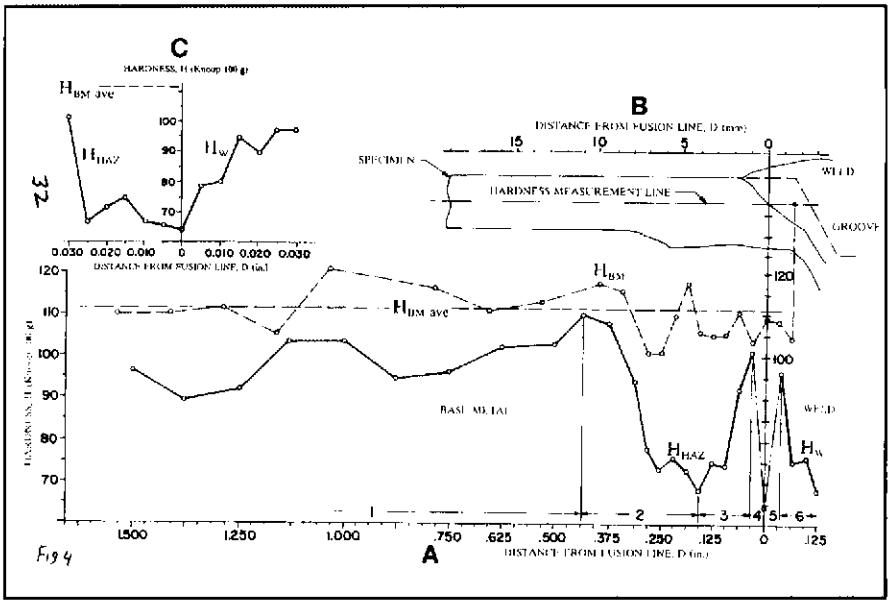

Fig. 4 — Typical hardness profile (Weld B17): A — hardness profile of unwelded base metal (HBM) and welded joint (H); B — actual cross-section of the welded joint; C — zoomed hardness profile at the weld interface (fusion line).

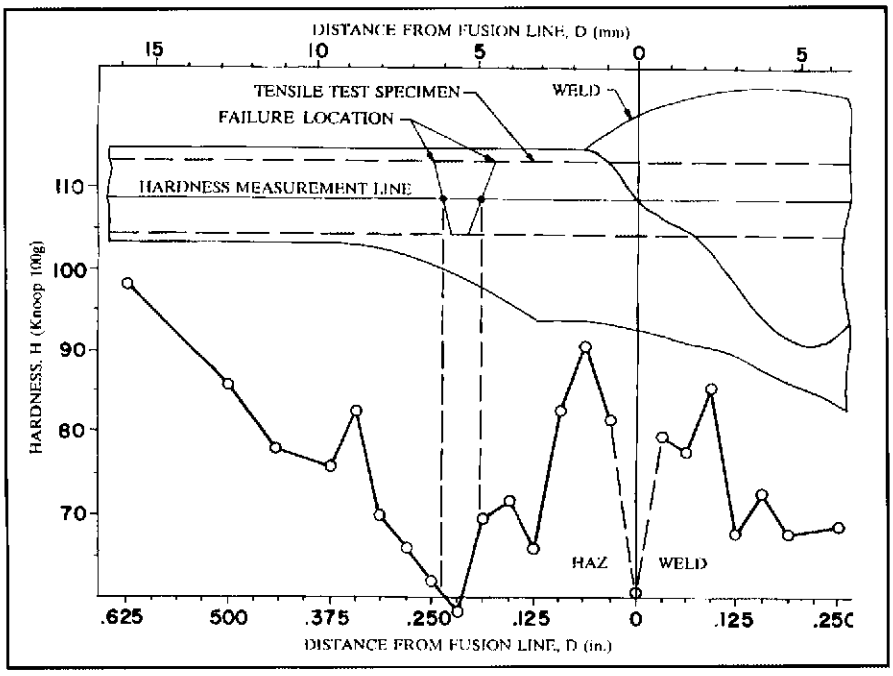

Fig. 5 — Effect of hardness on HAZ failure location in 6061-T6 tensile specimen (Weld B18).

imum and minimum hardness values (at the borders of the area) and W is the width of a particular hardness area.

The gradient of Area 2 ($G_{H2\ ave}$) appeared to be relatively low compared to other areas that are described later. The variations of $G_{H2\ ave}$ were within a range of 206 to 67 HK/in. (8.1–2.6 HK/mm) depending on Q. A significant hardness reduction in Area 2 indicates that profound changes in microstructure and properties had occurred in this area.

Area 3 is an area of a rapid hardness recovery. The degree of recovery varies from 72 to 100% of the $H_{BM\ ave}$. The width of the area (W_3) is typically narrower than W_2. Also, the dependence of W_3 on linear energy Q is not always as evident as that of Area 2. However, the effect of chilling of the HAZ is much stronger. For example, chilling of weld B17 reduced W_3, from 0.437 in. (11.1 mm) to 0.187 in. (4.8 mm), compared to its nonchilled counterpart Weld B16 performed under the same conditions. Hardness in Area 3 recovers at a much greater rate than hardness reduction in Area 2, based on the much higher hardness gradient (G_{H3}). G_{H3} varied in a range of 75 to 560 HK/in. (3.0–22.3 HK/mm). Such a dramatic hardness recovery may also indicate profound modifications of microstructure and properties within Area 3.

In the literature, Areas 2 and 3 are sometimes referred to as an "overaged zone." Although the term simplifies metallurgical reactions in this zone, the minimum hardness exhibited in this region results that on the border of Areas 2 and 3, there is a plane, parallel to the weld, of so-called HAZ weakness where a considerable loss of hardness and strength occurs. In fact, most of the tensile specimens tested in this study failed in the HAZ through this plane as will be discussed later.

Area 4 was found to be a very narrow layer, typically 0.031–0.062 in. (0.8–1.6 mm) wide, adjacent to the weld interface as schematically shown in Fig. 4A (phantom lines). The existence of this area has not been reported in prior literature. To reveal this area, microhardness measurements were taken at 0.005-in. (0.13-mm) increments. The actual hardness profile in this area has been rescaled and is shown in Fig. 4C. Within this area, H drops dramatically to a very low value, sometimes representing the lowest hardness across the joint. The lowest H value is typically on the weld interface and may be as low as 51 HK (45% $H_{BM\ ave}$). In contrast to the other areas, the width of Area 4 (W_4) does not seem to be influenced by linear energies Q or HAZ chilling. The hardness gradient (G_{H4}) is extremely high and may reach as high as 1194 HK/in. (47 HK/mm) for chilled specimens (B17, for example). These results indicate that almost half of the base metal hardness may be lost over an extremely narrow area of the HAZ, approximately 0.040 in. (1.0 mm) wide, immediately adjacent to the weld interface. Weld hardness on both sides of its center line shows a similar profile. The weld from the weld interface to the centerline may be divided in two typical hardness areas — Fig. 4A.

Area 5 was found to be a very narrow area adjacent to the weld interface on the side of the fusion zone. The existence of this area has not been reported in prior literature. Here, hardness dramatically increases, sometimes up to 92% $H_{BM\ ave}$ — Fig. 4C. The increase in hardness is extremely rapid. Most of the lost base metal hardness is restored within a distance of 0.010 to 0.020 in. (0.25–0.51 mm) from the weld interface. This corresponds to

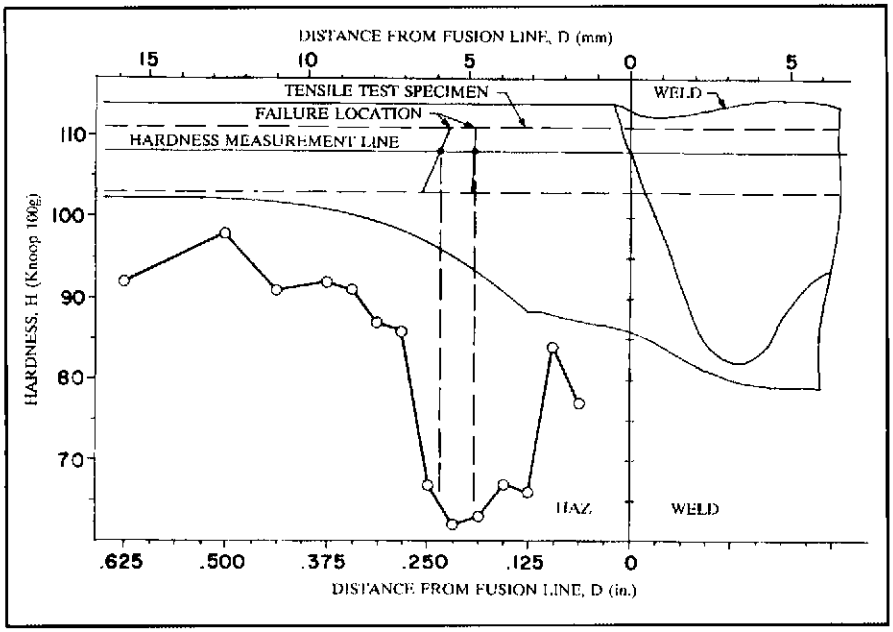

Fig. 6 — Effect of hardness on HAZ failure location in 6061-T6 tensile specimen (Weld C33).

an extremely high hardness gradient which may reach up to 3000 HK/in. (118 HK/mm).

Thus, Area 4 within the HAZ and Area 5 within the fusion zone create another plane of weakness that may facilitate failure of the welded joint. In this study, some of the tested tensile specimens failed through this plane.

Area 6 represents the remaining portion of the fusion zone up to the weld centerline. Here, H is gradually reduced toward the central portion of the weld where hardness values can be as low as 60 HK (54% $H_{BM\ ave}$). This indicates that the central portion of the weld may be vulnerable to failure, especially when gas porosity is present. In this study, several specimens failed within this area during tensile testing.

Hardness and Failure Location

The failure locations for some of the tested tensile specimens are summarized in Table 3. The results show that the tested specimens failed in three typical locations: within the HAZ, at the weld interface and within the weld fusion zone.

HAZ failure occurred at various distances (D_f) from the weld interface depending on the level of power (P) or linear energy (Q) utilized for welding and presence of HAZ chilling. D_f variations depended strongly on linear energy Q. The specimens that were produced at higher Q failed farther away from the weld interface than those performed at lower Q. Also, the failure appeared to be closer to the weld interface on the face side than on the root side of the tested specimen. Since hardness may serve as an indirect indication of tensile strength of the metal, attempts were made to correlate the failure locations with the hardness distributions across the joint as shown in Fig. 5. For this purpose, a cross-section of a welded joint was traced from its corresponding photograph (in this case B18 was taken as an illustration). A contour of the tensile specimen cut from this joint (outlined by dashed lines), the hardness measurement line and the failure location lines were accurately reconstructed for the traced welded joint. The corresponding hardness profile was superimposed on the welded joint using the same distance scale. The two failure lines indicate the variation in fracture path along the width of the specimen. The intersection points of the failure and hardness measurement lines represent a true failure location with relation to the hardness profile.

As it is evident from Fig. 5, the specimen failed through the plane of minimum HAZ hardness between Areas 2 and 3. The same phenomenon was consistently observed in all chilled and nonchilled specimens that failed in the HAZ with no regard to linear energy Q used for welding. For example, chilled Weld B18 (described above) was performed using high Q. Similar results were obtained for chilled Weld C33 performed using low Q (Fig. 6) and for nonchilled Weld B16 performed using medium high Q — Fig. 7.

Weld interface and weld failures were also observed in this study during testing of tensile specimens. As shown in Fig. 8 (Weld B17), the weld interface type of failure typically consisted of two fracture paths: 1) along the weld interface (or in the weld at a close proximity to the weld interface) at the root side (bottom) of the

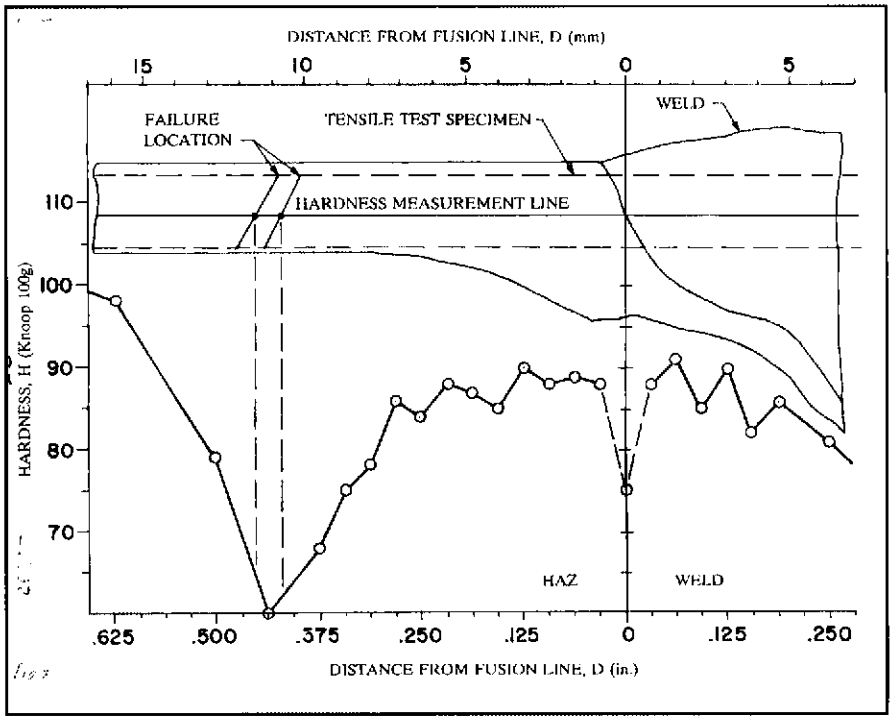

Fig. 7 — Effect of hardness on HAZ failure location in 6061-T6 tensile specimen (Weld B16).

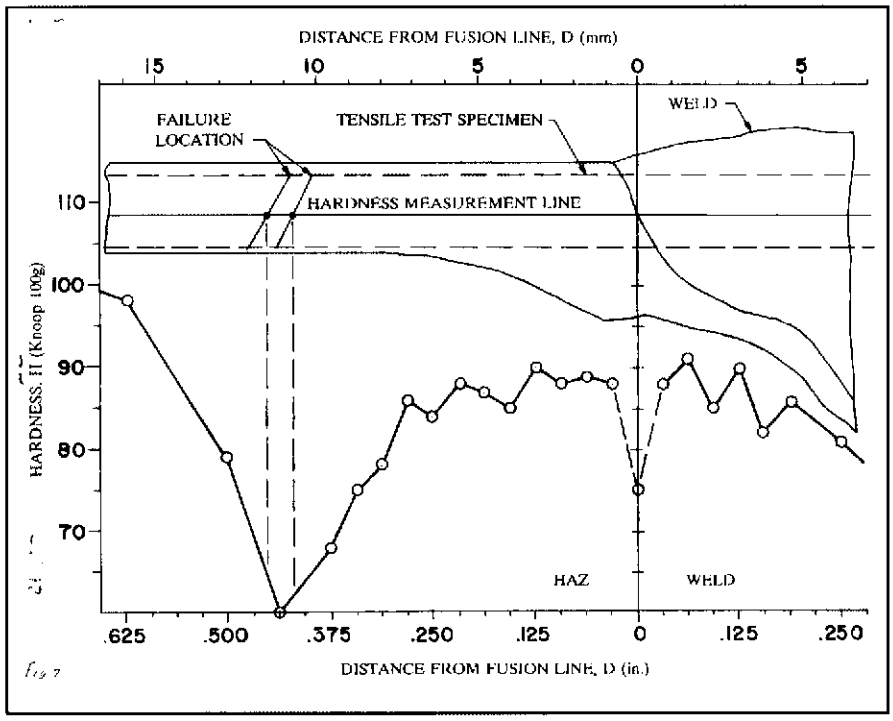

Fig. 8 — Effect of hardness on weld interface (fusion line) failure location in 6061-T6 tensile specimen (Weld B17).

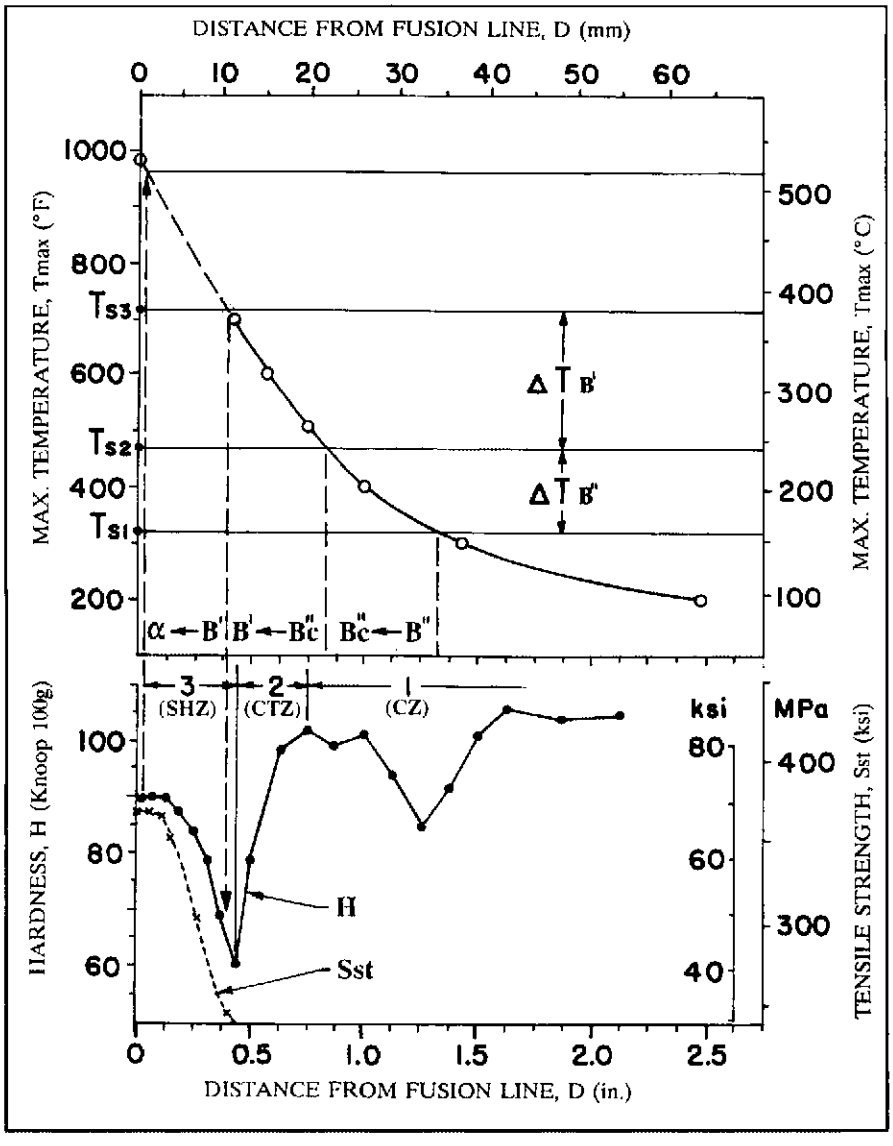

Fig. 9 — Peak temperature (T_{max}) and hardness (H) profiles in the HAZ (Weld B23).

specimen and 2) within the weld fairly away from the weld interface at the face side (top) of the specimen. It appeared that the failure initiated at the weld interface in the root area and propagated into the weld fusion zone. Thus, at the root of the welded joint, the failure is likely to occur through the plane of the minimum weld interface hardness and propagate into the softest area of the weld. Weld failure occurred rarely and typically in the middle portion of the weld that showed low hardness.

Thus the results of this experiment have proven that the specimen broken during tensile tests in the HAZ always fail through the plane of minimum HAZ hardness.

Hardness and Peak Temperatures in the HAZ

Based on the results of this study, it was found that there is a interrelationship between hardness (H) and peak temperatures (T_{max}) in the HAZ of the welded joint. It is illustrated in Fig. 9 for Weld B18 where H and T_{max} profiles across the HAZ superimposed on each other. The experimental and extrapolated points of the T_{max} profile are connected with solid and dashed lines, respectively. Solvus temperatures of the start of the B" phase formation T_{s1} (320°F) reported by Panceri, *et al.* (Ref. 7), the end of B"/the start of B' phases formation T_{s2} (464°F) reported by Miyauchi, *et al.* (Ref. 11), and the end of B' phase formation T_{s3} (716°F) reported by Miyauchi, *et al.* (Ref. 11), are indicated with the horizontal lines.

An important finding of this study was that, within the accuracy allowed by the experiments, the plane of the minimal hardness in the HAZ corresponds to solvus temperature T_{s3} (716°F), the upper temperature limit of the B' phase formation. This conclusion was confirmed by the analysis of the H-T_{max} relationships for many welds in this study with no regard to linear energy or chilling conditions used. For example, Fig. 9 described above was plotted for chilled Weld B18 performed at high linear energy Q. The same results were obtained for chilled welds B23 and B17 performed at low (Fig. 10) and medium-high (Fig. 11) linear energies Q, respectively. Thus, solvus temperature T_{s3} indicates the location of the softest (weakest) point of the HAZ.

Another important finding of this study was a clarification of the temperature range of a so-called "overaged zone." Burch (Ref. 14) studied the effect of AC GTAW on hardness of the HAZ of 6061-T4 aluminum alloy in the late 50s. He was the first to describe the overaged zone as the softest area of the welded joint located in the HAZ, where temperatures reach 570°–700°F (299°–371°C). The important conclusion of this study was that hardness Area 2 (Figs. 9, 10) in the HAZ spatially coincides with the temperature interval $\Delta T_{B'}$ of existence of the B' phase, which was defined by the range of 464°–716°F.

Thus, the clarification of the locations of the softest point and area in the HAZ are rather important since a hardness test is an inexpensive and readily available tool in practical applications. As will be shown later, knowledge of the location of the point of minimum hardness and the extent of the overaged zone may be very instrumental since it has certain correlation with tensile strength of the welded joints.

Discussion of Results

Relationship between Hardness and Microstructure in the HAZ

The results of the comprehensive analyses of hardness, peak temperatures and failure locations across the welded joint were discussed earlier in the current study. These analyses made it possible to speculate on the relationships between temperature, hardness and microstructures in the HAZ and at the weld interface of 6061-T6 alloy based on the background information on microstructural alterations in the HAZ of 6061-T6 welded joints available in literature.

The background data on this issue are scarce and scattered in literature. Despite a great number of publications on microstructures of Al-Mg-Si alloys, there are very few dedicated to investigation of the HAZ of welded joints.

Enjo and Kuroda (Ref. 9) studied HAZ microstructure in 6063-T5 commercial

alloy after GTA welding (1.03 kJ/mm, 26.16 kJ/in.) using methods of electrical resistivity and transmission electron microscopy (TEM). The results of hardness measurements (Vickers, 300-g load) were correlated with resistivity data plotted as function of distance (D) from the weld interface. The data were verified by TEM micrographs. In the HAZ, at D = 15–40 mm, (0.59–1.57 in.), the authors identified an area similar to that described in the present study as Area 1 — Fig. 4A. Here, however, hardness was slightly higher than that of as-received 6063-T5 material due to somewhat higher content of B″ phase in this area. In an area similar to Area 2 (D = 10–14 mm; 0.39–0.55 in.), a drastic reduction in hardness (from 80 to 50 HV) occurred. This was attributed to a significant reduction (from 62 to 8%) of B″ phase due to its "dissolutioning." At the same time, increase of B′ phase (from 5 to 14%) was observed. Areas 3 and 4 were not revealed by the authors, but it was reported that hardness at D = 0–10 mm (0–0.39 in.) was slightly decreased (from 50 to 45 HV) in the direction of the weld interface.

Dumolt (Ref. 3) studied the HAZ formed after GTA welding (0.65 kJ/mm; 16.6 kJ/in.) in 6061 alloy. Prior to welding, the alloy was heat treated to T6-temper to precipitate B″ phase. In that study, hardness (Rockwell, F scale) was correlated with peak HAZ temperatures (T_{max}) plotted as a function of distance (D) from the weld interface. The data were verified by TEM micrographs. Dumolt identified Area 2 (Fig. 4A) and observed that B″ particles started to grow (to coarsen) at the beginning of Area 2 (T_{max} = 300°C/572°F) resulting in hardness reduction. As coarsening continued, B″ phase started to transform into B′ phase in the middle of Area 2 (T_{max} = 345°C/653°F). Both processes continued gradually until the end of Area 2 (T_{max} = 460°C/860°F), resulting in a significant drop in hardness. Thus, according to Dumolt, coarsening of B″ phase and its transformation into B′ phase are responsible for softening in Area 2. Also, Dumolt identified Area 3 where hardness began to grow. In this area, dissolutioning of B′ phase was observed resulting in "solid solution hardening from that point to the edge of the fusion zone." Area 4 was not recognized, although slight hardness reduction close to the weld interface above T_{max} = 500°C (932°F) was observed. This was attributed to the large diameter (0.062 in.; 1.6 mm) of the indenter used which could include the "soft fusion zone." Above 500°C, no B″ or B′ precipitates were observed.

A microstructural profile of the HAZ of the welded joint in 6061-T6 alloy is

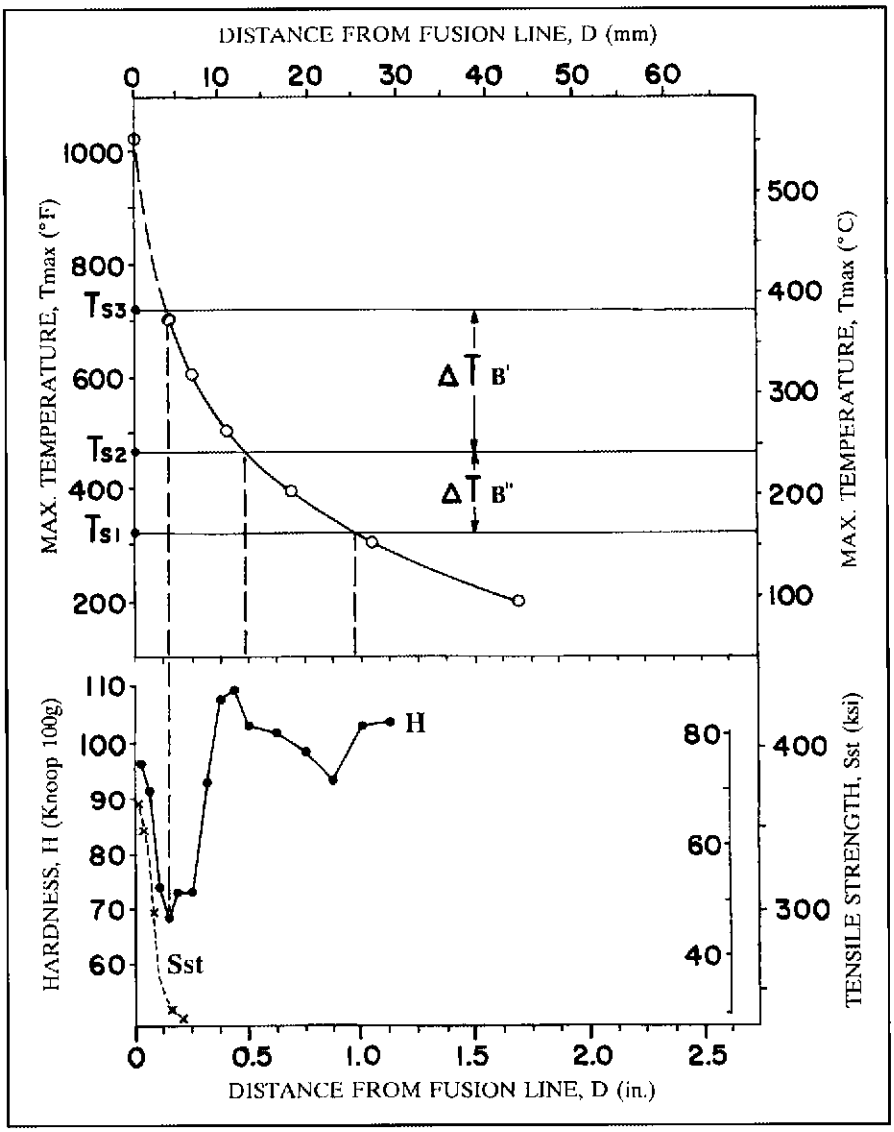

Fig. 10 — Peak temperature (T_{max}) and hardness (H) profiles in the HAZ (Weld B18).

described in Fig. 12 based on the results of the studies described above (Refs. 9, 3) and the current study. In Fig. 12, the H and T_{max} profiles across the HAZ superimposed on each other corresponding to nonchilled weld B16 performed at medium-high linear energy.

Area 1 is characterized by local soft spots and lower average hardness compared to the base metal. According to (Ref. 3), Alloy 6061-T6 is heat treated to precipitate B″ phase to achieve its maximum tensile properties and hardness. As Fig. 12 shows, Area 1 is subjected to temperatures below 482°F (250°C). This temperature is lower than that reported by Dumolt (Ref. 3) for the start of a widespread coarsening of the B″ phase in the HAZ (572°F). However, local spots of the coarsening B″ particles are likely to occur since Area 1 is located within the ΔT_B temperature range (320°–464°F), the interval of the existence of the B″ phase. Also, the metal may be held at the temperature a relatively long time during cooling.

Thus, hardness Area 1 may represent the location of a structural zone where local accumulations of coarsened B″ phase are likely to appear in the HAZ. The presence of this structural zone indicates the first signs of microstructural changes to occur in the HAZ of 6061-T6 alloy. This means that the present notion about the extent of the HAZ in 6061-T6 alloy may need to be reviewed. To facilitate the further discussion, this structural zone will be referred to as the coarsening zone (CZ).

Area 2 is characterized by a significant reduction in hardness as the weld interface approaches — Fig. 12. This was established by Burch (Ref. 14) and other researchers, and confirmed by the current study. In the current study, it was found that hardness Area 2 spatially co-

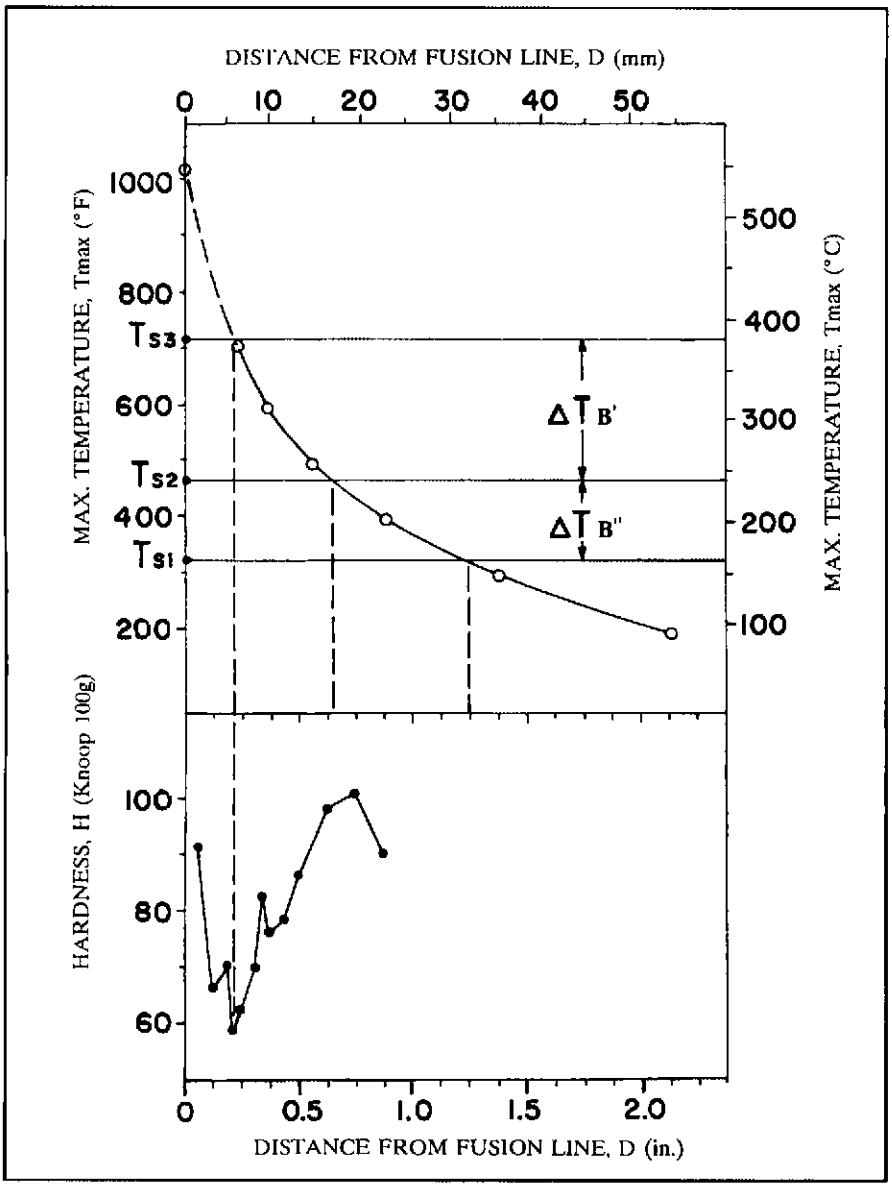

Fig. 11 — Effect of peak temperature (T_{max}) profile on hardness (H) and microstructure in the HAZ of 6061-T6 welded joint (Weld B16).

incides with the temperature interval ($\Delta T_{B'}$) of the existence of the B′ phase which is 240°–380°C (464°–716°F). Also, the solvus temperature T_{s3} (380°C; 716°F) of this interval corresponds to the location of the point of the minimal hardness in the HAZ, as was discussed earlier. Dumolt (Ref. 3) observed two simultaneous processes to occur in Area 2: coarsening of the B″ phase and its transformation into B′ phase, despite the fact that the T_{s3} temperature (860°F) observed by Dumolt was higher than that reported by both Miyauchi, *et al.* (Ref. 11), and the current study. Enjo and Kuroda (Ref. 9) also observed transformation of the B″ phase into B′ phase in Area 2.

Thus, based on the prior and current studies, hardness Area 2 is believed to represent the location of a structural zone where coarsening of B″ phase and its transformation into B′ phase is likely to occur in the HAZ of 6061-T6 alloy. To facilitate the further discussion, this structural zone will be referred to as the coarsening-transformation zone (CTZ). Also, the solvus temperature T_{s3} indicates the point in the CTZ where the size of B″ particles and the content of B′ particles reach the maximum, while strength of the welded joint is reduced to a minimum.

Area 3 is characterized by an increase in hardness as the weld interface approaches — Fig. 12. This was established by Dumolt (Ref. 3) and confirmed by the current study. Dumolt observed two simultaneous processes to occur in Area 3: 1) dissolutioning of the B″ and B′particles until no precipitates were observed close to weld interface above 932°F; and 2) solid solution hardening responsible for an increase in hardness. Dissolution of the precipitates occurs since the particles are held at temperatures higher than T_{s3} during heating and cooling as a result of welding. Dissolutioning process enriches the solid solution of the aluminum matrix with Si and Mg. This increases hardness and strength. The closer the metal to the weld interface, the higher the temperature, the higher the amount of precipitates dissolved, and the higher the hardness and strength.

The fact that such a dramatic strength recovery is possible over such a small area of the HAZ subjected to high heating and cooling rates can be confirmed from the solution-hardening heat treatment practice of another age-hardenable alloy, 2014-T6. It is known (Ref. 15) that solution temperature (T_{s1}) has a significant effect on tensile strength (S_{st}) of 2014 alloy treated to T6-temper. The graphic data taken from Ref. 15 describing S_{st} as function of T_{s1} were replotted in Figs. 9 and 10 over the hardness profiles (short dashed lines). It is obvious that the tensile strength curves follow those of hardness in Area 3.

Thus, hardness Area 3 may represent the location of a structural zone where dissolution of B″ and B′ phases occurs. In this respect, this zone may be called the solution-hardening zone (SHZ).

A microstructural profile of the transition zone, the area immediately adjacent to the weld interface, has not been reported in prior literature. In this study, very narrow hardness areas (Areas 4, 5) were found on both sides of the weld interface, as shown in Fig. 4A. Hardness in Area 4 (HAZ) exhibits a surprising dramatic reduction and then recovers even more rapidly in Area 5 (weld). The temperatures (T_{max}) achieved in Area 4 are above 500°C and reach the melting point of the alloy at the weld interface. According to Dumolt (Ref. 3), there were no precipitates (B″ or B′) found in the area next to the weld interface where T > 500°C due to their dissolution in the aluminum matrix. In other words, the aluminum matrix (α′) is enriched with Mg and Si, the elements lending strength to the alloy. Nevertheless, a significant loss of strength in Area 4 is evident. There are possibly two reasons for this phenomenon.

The first one is heat treatment of the metal in Area 4. In fact, the instant temperature gradients during heating and cooling of this area are so high that the metal may undergo treatment approaching solutioning and quenching. However, additional experiments showed that such treatment alone can not reduce hardness that low (down to 51 HK). The specimens cut from the unwelded panels

were subjected to solutioning heating similar to that used for T6-temper (990°F; 532°C for 1 h). To produce the softest possible metal, the specimens were quenched in cold water. Hardness was taken as soon as possible (within 4 h) to avoid excessive hardening due to natural aging. Despite all this, the minimum hardness recorded was only 76 HK. It is obvious that after three weeks of aging (used in the current study) hardness would have been even higher. Thus, solutioning and quenching alone cannot be responsible for a significant loss of strength in Area 4.

A possible co-contributor to the phenomenon observed in Areas 4 and 5 could be redistribution of strengthening alloying elements (Mg and Si) across the weld interface. So called "heterogenous" diffusion described by Malin (Ref. 16) may affect the molten weld and solid base metals adjacent to the interface between the liquid and solid phases. The reason for this is that some alloying elements, including Mg and Si, have higher solubility in liquid than solid phases. As was shown by Petrov (Ref. 17), during the interaction of solid and liquid phases, migration of such an element from solid to liquid phase may occur in the partially melted zone limited by liquidus and solidus temperatures. The character of redistribution of such element is schematically shown in Fig. 13. This fact indicates that after solidification, the partial melting area adjacent to the solidus may be depleted with Mg. Loss of Mg may result in reduction of hardness and strength at the weld interface on the side of the HAZ. This process may be facilitated by the concentration gradient between the solid base and the liquid weld metals. In fact, for 6061 alloy and 4043 welding wire compositions (Table 1) and the rate of dilution 20–60% (Table 2), it is likely to expect about 0.2–0.5% Mg in the weld vs. 0.85% Mg in the base metal. Silicon may also migrate into the weld, despite the fact that migration of Si goes against the concentration gradient (4.0–1.4% Si in the weld vs. 0.68% Si in the base metal). Losses of Mg and possibly Si may result in losses of hardness and strength in the partial melting area adjacent to the solid metal. On the other hand, in the area of partial melting adjacent to the liquidus, a concentration peak of Mg may occur which exceeds that in the weld making the metal age-hardenable. The scenario described above is possible. Comparison of the hardness curve in Areas 4 and 5 (Fig. 4A) with that in Fig. 13 shows that both curves have similar profiles. In this respect, these areas may be called the transition zone (TZ).

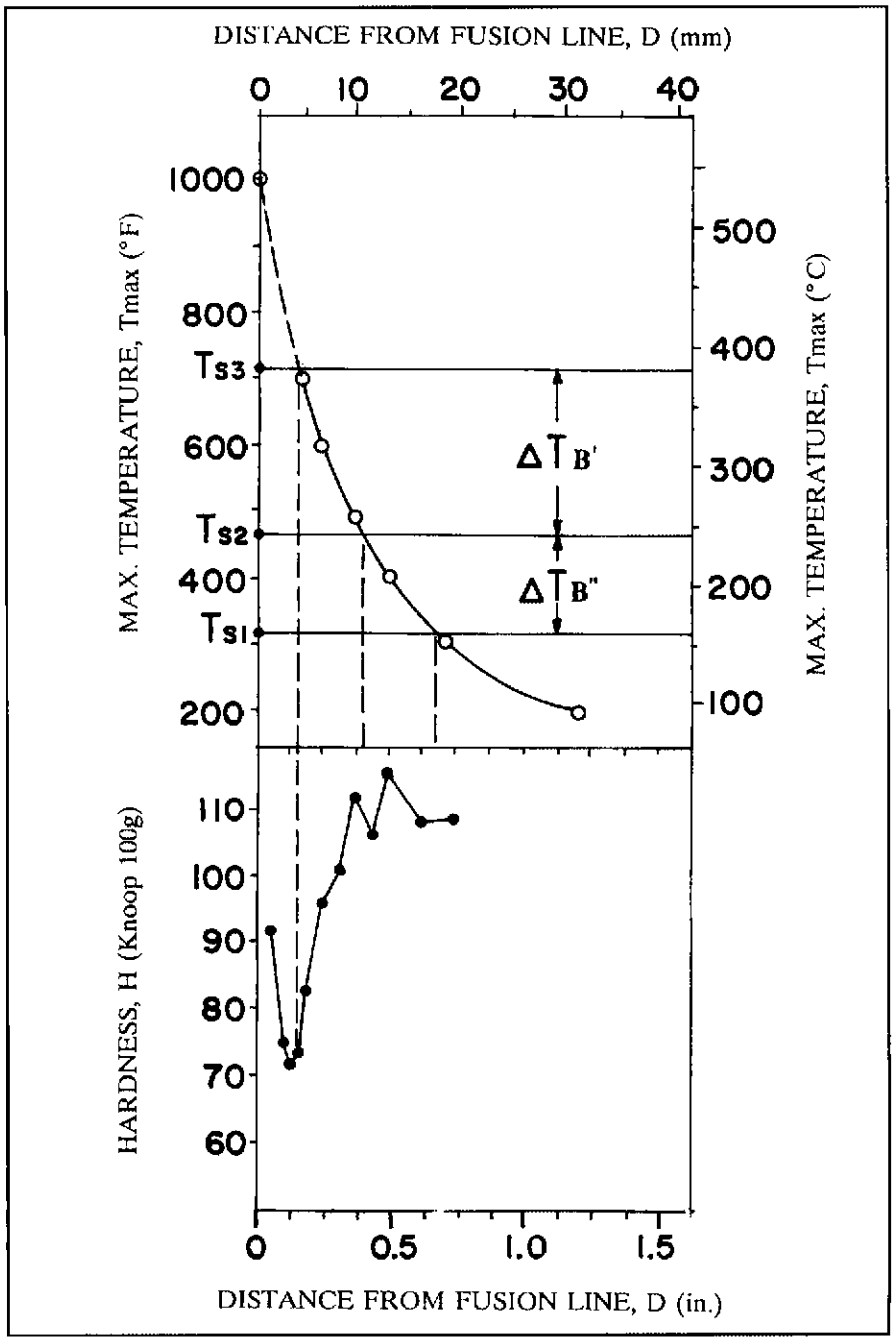

Fig. 12 — Peak temperature (T_{max}) and hardness (H) profiles in the HAZ (Weld B17).

Relationships between Temperature, Hardness and Strength

The results of this study showed the effects of variations in welding variables on thermal conditions of the HAZ in 6061-T6 alloy during welding. As a result, the HAZ metal subjected to elevated temperatures was adversely affected resulting in the reduction of hardness and tensile strength of the welded joints. To explain these phenomena, the attempt was made to analyze the detrimental alterations of the initial microstructure in the HAZ using data available in literature. The main objective of the following discussion is, by analyzing the relationships between HAZ temperatures, microstructure, hardness and strength, to establish simple criteria based on temperature or hardness measurements to qualitatively predict the tensile strength of the welded joints. To facilitate and simplify the discussion, several useful definitions are presented below.

The critical temperature interval ΔT_{cr} is the peak temperature range of 464° to 716°F, which is the temperature interval

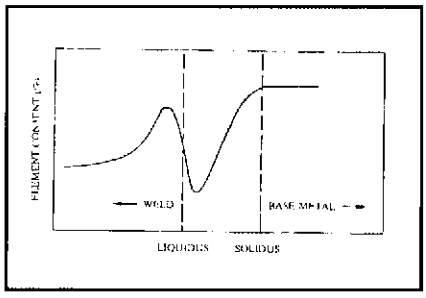

Fig. 13 — Schematic representation of migration of an element with higher solubility in liquid phase through a partially melted zone between weld and base metal (Ref. 17).

of B′ phase formation ($\Delta T_{B'}$) in the HAZ. The critical zone (CTZ) is an area of the HAZ heated within the critical temperature interval ΔT_{cr} where a significant reduction of hardness occurs. The critical temperature T_{cr} is the temperature of 716°F at which hardness is reduced to a minimum. The width of the critical zone will be designated W_{cr}.

Analysis of numerous hardness profiles and tensile strengths of the corresponding welded joints performed under various welding conditions showed that there is a certain correlation between hardness and strength. As was found in this study, the average hardness gradient $G_{H2\ ave}$ may be used as an indicator of strength of the welded joints. This is illustrated in Fig. 14A, where $G_{H2\ ave}$ values, determined for welds C33, C35 and C30 (failed in the HAZ), and the welds' average tensile strength (S_t) are plotted as function of linear energy Q. It is evident that both curves follow the same trend. The extremes on both curves may indicate that the effect of arc heat on the base metal is reversed at some point. Redistribution of heat between that consumed for base metal melting and that consumed for heating of the HAZ is illustrated in Fig. 14A, where the dilution rate (DR) is plotted for the same welds. Dilution is known as a direct indicator of the melting (penetration) efficiency of the arc. As seen in Fig. 14A, the dilution curve shows the same trend as those of hardness and strength.

The temperature field may be characterized by the peak temperatures (T_{max}) reached at various points of the HAZ. According to Adams (Ref. 18), under equal conditions, at a given point of the HAZ, T_{max} depends on linear energy Q and the distance D from the weld interface as was illustrated in Figs. 9–12. Since T_{max} varies across the width of the critical zone W_{cr}, the average peak temperature gradient $G_{TCTZ\ ave}$ will be introduced as a criterion characterizing the intensity of the temperature field in the critical zone, as follows:

$$G_{T\ CTZ\ ave} = \Delta T_{cr} / W_{cr}$$

Since ΔT_{cr} is constant, W_{cr} may serve as a convenient qualitative criterion as well. Figure 14B (solid line) shows $G_{T\ CTZ\ ave}$ as a function of linear energy Q plotted for chilled Welds B23, B22, B17 and B18. The graph shows that with increase in linear energy Q, the critical peak temperature gradient $G_{TCTZ\ ave}$ is decreased. The same relationship is observed for the hardness gradient $G_{H2\ ave}$ plotted in Fig. 14B (dashed line) for the same welds. It is obvious that there is a direct linear correlation between both gradients.

Thus, the following conclusions may be drawn from the discussion above: The average hardness or peak temperature gradients, or the width (W_{cr}) of the critical zone (CTZ) may serve as qualitative criteria of strength of the welded joint. The higher the gradients or the lower the width of the critical zone, the higher the hardness and strength.

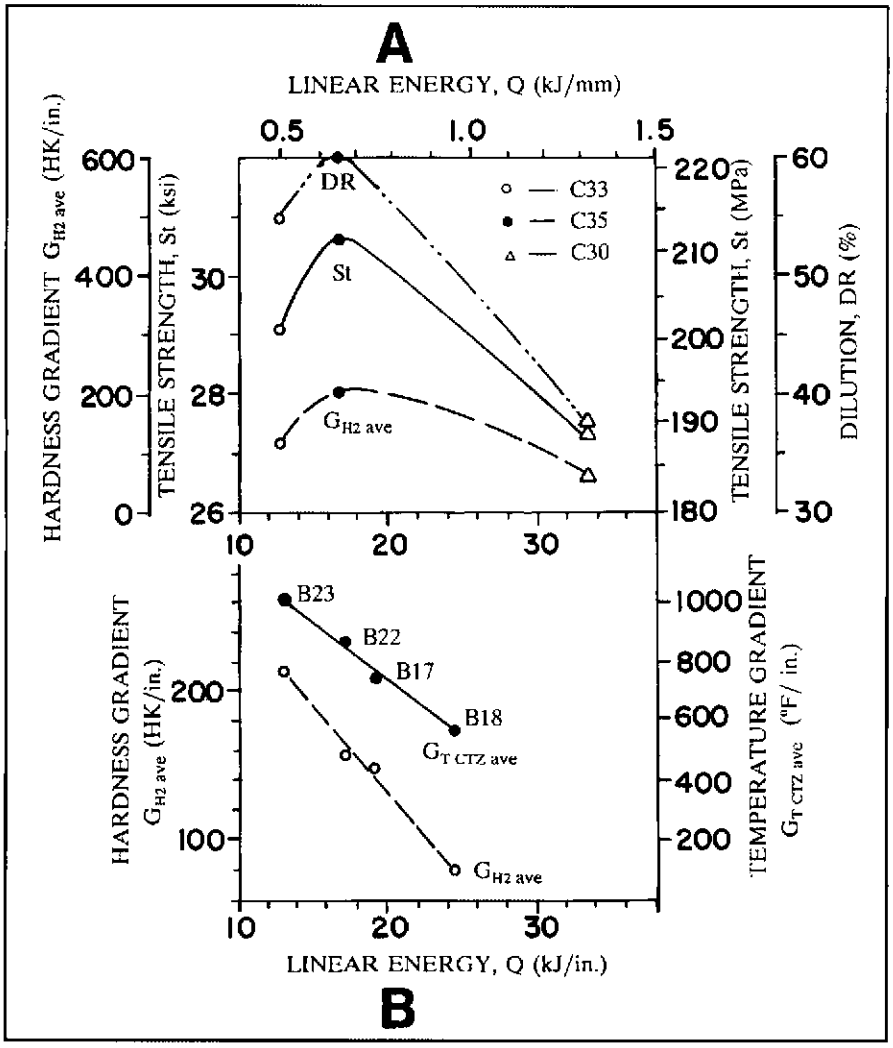

Fig. 14 — Relationship between temperature, hardness and strength in 6061-T6 welded joints. A — Effect of peak temperature gradient (GT CTZ) in the "critical" zone on hardness gradient (GH2); B — relationship between hardness gradient (GH2), strength (St) and dilution (DR).

Effect of Linear Energy on Width and Location of the Critical Zone

Two main factors are believed to be responsible for loss of hardness and strength in the critical zone: the extent of the zone and the time of exposure to critical temperature interval ΔT_{cr} (464°–716°F). The current study showed that the intricate relationships exist between the linear energy (Q), the peak temperature (T_{max}), exposure time (t) at ΔT_{cr}, the width of the critical zone (W_{cr}), the distance (D) of the point where the critical temperature T_{cr} (716°F) is reached from the weld, and strength of the welded joints.

The effect of linear energy on the width and location of the critical zone is illustrated in Fig. 15A and B. At constant linear energy, a moving arc creates a temperature field in the HAZ which is called "quasi-stationary" field. The term implies that the field is moving along the joint, but remains unchanged relative to the space coordinates moving along with the

arc, except for transient conditions observed, for example, at weld start or termination. In Fig. 15B, the arc with the center in point K is moving along the weld axis in the direction of welding indicated by the arrow. It produces the temperature field, which is schematically represented by the contour of the weld pool (fat lines) and two "critical" isotherms, 716° and 464°F. Two sets of isotherms are presented: for high-linear energy Q_1 (right side) and low-linear energy Q_2 (left side).

As the isotherms (on the right side) move forward, the base metal at point A, (464°F) can be viewed as if it is moving backward relative to the arc along the dashed line A_1C_1 as shown by the arrow. The temperature of the metal increases, as it intersects the isotherms of higher temperature, until it reaches T_{max} = 716°F at point B_1. Then the metal cools off to 464°F again when it reaches point C_1. A similar thermal cycle is repeated for the base metal located at any intermediate point. For example, point A_1 reaches $T_{max} = T_1$ at point B_1. The critical isotherms shown on the left side of the weld axis in Fig. 15B correspond to lower linear energy. According to Ref. 19, narrower and shorter isotherms are produced at low-linear energy since the temperature gradient is higher. The graphs, which schematically represent T_{max} as a function of distance (D) from the weld interface, are shown in Fig. 15A. They also show the critical zone (W_{cr}) subjected to temperatures within the critical temperature interval (ΔT_{cr}). Comparing the graphs on both sides of the weld axis, it is evident that at high-linear energy Q_1, the distance D_1 from the weld interface to the point B_1 (where the critical temperature T_{cr} = 716°F is reached) is smaller than the distance D_2 of the similar point B_2 at low-linear energy Q_2. Also, at high Q_1, the width of the critical zone (W_{cr1}) is greater than that (W_{cr2}) at low Q_2.

The effect of linear energy on the time of exposure of the critical zone is illustrated in Fig. 15B and C. The base metal at point A_1 is moving along the dashed line A_1C_1 with a constant speed S. This means that the travel distance L, represents time (t) of exposure to temperatures within the critical temperature interval ΔT_{cr} and can be calculated as follows:

$$t = L_1/S$$

This includes the time of heating from 464° to 716°F and consequent cooling again to 464°F represented by travel distances A_1B_1 and B_1C_1, respectively. The same considerations are applicable to all the intermediate isotherms within ΔT_{cr} (points A_i, B_i and C_i, for example). The times (t) of exposure to temperatures within ΔT_{cr} as a function of distance (D)

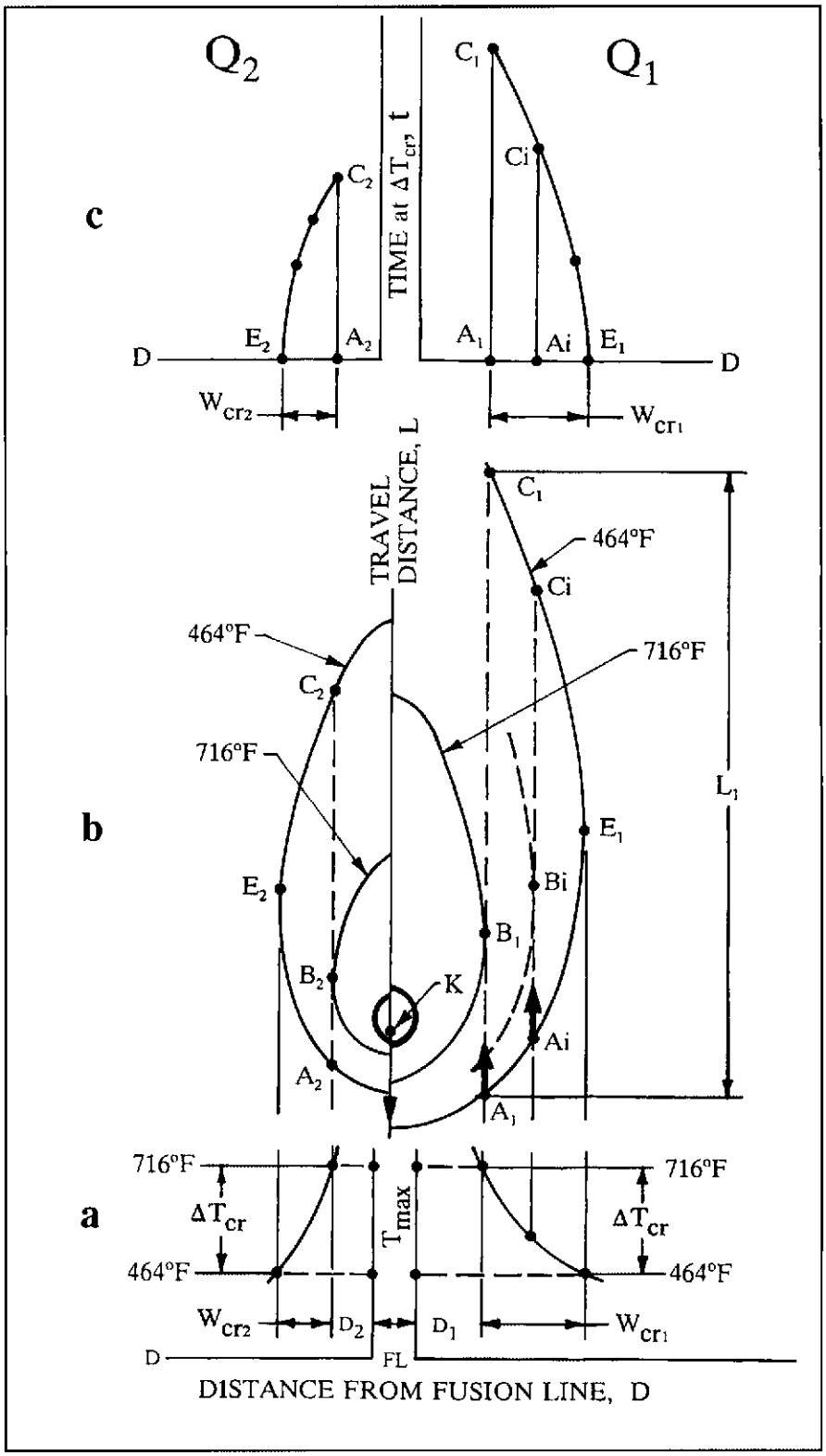

Fig. 15 — Schematic representation of the isotherms of a thermal cycle (b), and maximum temperature Tmax (a) and exposure time (c) as functions of distance D from the weld interface (fusion line). Legend: Wcr — width of the "critical" zone; ΔTcr — "critical" temperature interval; K center of the arc; fat lines — weld pool; linear energy levels: high — Q1 (right side), low — Q2 (left side).

from weld interface are shown in Fig. 15C for high-linear energy Q, (right side) and low-linear energy Q_2 (left side). Comparing the graphs, it is evident that at high Q_1, the point A_1 is exposed longer (corresponds to distance A_1C_1) to critical temperature T_{cr} = 716°F than the similar point A_2 (corresponds to distance A_2C_2) at low-linear energy Q_2.

Thus, the relationships described above can be summarized as follows: The higher the linear energy Q, the wider the critical zone and the longer time it is exposed to temperature of the critical temperature interval ΔT_{cr}. The wider the critical zone, the greater number of the B″ particles become coarse loosing their initial strength. The longer the time of exposure, the coarser the B″ particles become and the larger number of these particles is transformed into less stronger B′ phase precipitate in the critical zone.

A discriminating strength test was developed in the current study based on the correlation between strength of the welded joints in 6061-T6 alloy and the width/location of the critical zone in the HAZ. The test allows the different welding conditions to be discriminated in terms of strength by a simple comparative procedure. For this purpose, two strips of liquid temperature paints (380° and 240°C) should be applied across the welded joints to be compared. After welding, by measuring the difference in lengths of molten portions of the strips from the weld edges, the widths of the critical zones can be determined. The weld with the shortest critical zone and located at the closest distance from the weld will be stronger.

Conclusions

Relationships were investigated between welding variables, peak temperatures, microhardness, dilution, microstructure, failure location and strength of GMA welded joints in extruded aluminum Alloy 6061-T6 in the HAZ and at the weld interface (fusion line).

Comprehensive hardness tests were conducted across the welded joint where five typical hardness zones were experimentally identified.

A plane exhibiting minimum hardness was detected within the HAZ and was responsible for the majority of failures during tensile testing.

Another plane exhibiting very low hardness was unexpectedly revealed in a very narrow area, less than 0.020 in. (0.5 mm) wide immediately adjacent to the weld interface. Some of the failures during tensile testing occurred in this region.

Peak temperatures profiles were measured in the HAZ and compared with corresponding hardness profiles.

It was found experimentally that the minimum hardness and the location of failure of the tensile specimens in the HAZ is located at the point subjected to a temperature of 716°F (380°C). This is the upper limit of existence of B′ phase, the main strengthening precipitate in Alloy 6061-T6.

The greatest effect on hardness and strength of the welded joints was found to be in a critical zone of the HAZ (sometimes called overaged zone in literature) subjected to peak temperatures of 464° to 716°F (240°–380°C), the temperature interval ($\Delta T_{B'}$) of existence of the B′ phase precipitate.

A direct relationship between average peak temperature gradient and average hardness gradient in the critical zone was established. Both gradients have direct correlation with strength of the welded joints. The lower the gradients, the lower the tensile strength.

Two main factors were identified which are responsible for loss of hardness and strength in the critical zone: the extent of the zone and the time of its exposure to the critical temperature interval $\Delta T_{B'}$ (464° -716°F).

It was found that the strength of the welded joints of Alloy 6061-T6 can be qualitatively determined by the width and location of the critical zone. The narrower the critical zone and the closer this zone to the weld, the higher the strength of the welded joint.

A comparative practical test was developed to discriminate welding conditions by determining the width and the location of the critical zone using temperature paints or sticks.

The losses of hardness and strength in the HAZ are believed to be a result of coarsening of strengthening B″ phase precipitate and its transformation into B′ phase. The loss of hardness and strength in the transition zone at the weld interface may be a result of a complete dissolution of the precipitates and migration of Mg from the base metal into the weld.

Acknowledgments

Support for this research program was provided by the U.S. Army, Belvoir Research Development and Engineering Center, Bridge Division, under contract No. DAAK70-88-C-0024 and Electro-Com GARD. Special thanks go to D. J. Hogan for his assistance in experimentation and T. Sajdak for preparation of the manuscript.

References

1. Malin, V. Y. 1969. Investigation of brittle fine layers along fusion line between low-carbon base metal and Cr-Ni weld in welding of clad steels. *Obrabotka Metallov Davieniem* (Metal Working), Transactions of Leningrad Polytechnical Institute, No. 308, Mashinostroenie Publishing House, Leningrad, pp. 197-204.

2. Ceresara, S., DiRusso, E., Fiorini, P., Giarda, A. 1969-1970. Effect of Si excess on the aging behavior of Al-Mg_2Si 0.8% alloy. *Mater. Sci. Eng.*, Vol. 5, pp. 220-227.

3. Dumolt, S. D. 1983. An investigation of the microstructural changes in heat-affected zone of age-hardenable aluminum alloys using transmission electron microscopy. Ph.D. Thesis, Carnegie-Mellon University, Pittsburgh, PA.

4. Suzuki, H., Kanno, M., Shiraishi, Y., and Hanawa, K. 1979. Effects of copper addition on aging phenomena in Al-Mg-Si alloys. *J. Japan Inst. of Light Metals*, Vol. 29, pp. 575-581.

5. Mondolfo, L. F. 1976. *Aluminum Alloys: Structure and Properties*. Butterworths, pp. 644–651.

6. *Ibid.* pp. 566–572.

7. Panseri, C., and Federighi, T. 1966. A resistometric study of precipitation in an aluminum 1.4% Mg_2Si alloy. *Journal of Institute of Metals*, Vol. 94., pp. 94–107.

8. Lutts, A. 1961. Pre-precipitation in Al-Mg-Ge and Al-Mg-Si. *ACTA Metallurgica* 9 (6): 577–586.

9. Enjo, T., and Kuroda, I. 1982. Microstructure in weld heat-affected zone of Al-Mg-Si alloy. *Transaction of JWRI* 11(1): 61–66.

10. Thomas, G. 1961–62. The aging characteristics of aluminum alloys. *Journals of Institute of Metals*, Vol. 90, pp. 57–63.

11. Miyauchi, T., Fujikawa, S., Hirano, K. 1971. Precipitation process of Al-Mg-Si Alloys by Aging. *Journal of Japan Institute of Light Metals* 21(9): 595.

12. Miyazaki, M., Nishio, K., Katoh, M., Mukae, S. and Kerr, W. 1990. Quantitative investigation of heat-affected zone in aluminum alloy A6061. *Welding Journal* 69 (9): 362–371.

13. Kou, S. 1986. Welding metallurgy and weldability of high-strength aluminum alloys. Welding Research Council, New York, Bulletin 320, p. 8.

14. Burch, W. I. 1958. The effect of welding speed on strength of 6061-T6 aluminum joints. *Welding Journal* 37(8): 361–367.

15. Hatch, J. E. 1984. *Aluminum: Properties and Physical Metallurgy*. Aluminum Association, Inc., published by ASM, Materials Park, Ohio, p. 153.

16. Malin, V. Y. 1968. Migration of carbon from low-carbon base metal into Cr-Ni weld during contact of liquid and solid metal phases. *Mashinostroenie* (Machine Building), Transactions of Leningrad Polytechnical Institute, No. 299, Mashinostroenie Publishing House, Leningrad, pp. 289–294.

17. Petrov, G. L. 1963. Non-uniformity of metal of welded joints. *Sudpromgiz*, Leningrad, pp. 56–62.

18. Adams, C.M. Jr. 1958. Cooling rates and peak temperatures in fusion welding. *Welding Journal* 37 (5): 210–215.

19. Paton, B. E. 1974. Technology of electrical fusion welding of metals and alloys. *Mashinostroenie*, Moscow, p. 61, 62.